

# Refined Temporal Pyramidal Compression-and-Amplification Transformer for 3D Human Pose Estimation

Hanbing Liu<sup>1,2\*</sup>, Wangmeng Xiang<sup>2\*†</sup>, Jun-Yan He<sup>2\*</sup>, Zhi-Qi Cheng<sup>3\*</sup>,  
Bin Luo<sup>2</sup>, Yifeng Geng<sup>2</sup>, Xuansong Xie<sup>2</sup>

<sup>1</sup>Tsinghua University,

<sup>2</sup>DAMO Academy, Alibaba Group,

<sup>3</sup>Carnegie Mellon University

liuhb21@mails.tsinghua.edu.cn, zhiqi@cs.cmu.edu,

{wangmeng.xwm, leyuan.hjy, luwu.lb, cangyu.gyf}@alibaba-inc.com, xingtong.xxs@taobao.com

## Abstract

Accurately estimating the 3D pose of humans in video sequences requires both accuracy and a well-structured architecture. With the success of transformers, we introduce the **Refined Temporal Pyramidal Compression-and-Amplification (RTPCA)** transformer. Exploiting the temporal dimension, RTPCA extends intra-block temporal modeling via its Temporal Pyramidal Compression-and-Amplification (TPCA) structure and refines inter-block feature interaction with a Cross-Layer Refinement (XLR) module. In particular, TPCA block exploits a temporal pyramid paradigm, reinforcing key and value representation capabilities and seamlessly extracting spatial semantics from motion sequences. We stitch these TPCA blocks with XLR that promotes rich semantic representation through continuous interaction of queries, keys, and values. This strategy embodies early-stage information with current flows, addressing typical deficits in detail and stability seen in other transformer-based methods. We demonstrate the effectiveness of RTPCA by achieving state-of-the-art results on Human3.6M, HumanEva-I, and MPI-INF-3DHP benchmarks with minimal computational overhead. The source code is available at <https://github.com/hbing-l/RTPCA>.

## Introduction

Deep learning architectures for 3D human pose estimation have witnessed exponential growth and success over the years (Gong, Zhang, and Feng 2021; Zhao, Wang, and Tian 2022; Zheng et al. 2021; Hassanin et al. 2022; Hu et al. 2021; Zhang et al. 2022; Cheng et al. 2022; He et al. 2021a; Tu et al. 2023; Hauptmann et al. 2023). Notable strides have been made using body joint representations (Zhou et al. 2022, 2023), human pose priors (Zhao, Wang, and Tian 2022; Hu et al. 2021; Liu et al. 2023), and establishing spatio-temporal relationships among frames (Zhang et al. 2022). The wave of transformer-based attention mechanisms, specifically the Vision Transformer (ViT) (Dosovitskiy et al. 2021; Chen, Fan, and Panda 2021; Chen et al. 2023), has shown substantial promise in unraveling patch-based spatial relationships crucial for 3D pose estimation.

\*These authors contributed equally.

†Corresponding author.

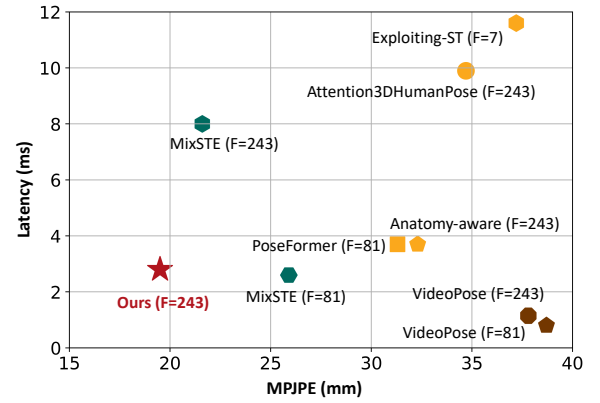


Figure 1: **Comparison on the Human3.6M dataset to evaluate the performance of various methods in terms of MPJPE and latency.** Here the performance closer to the origin of the coordinates is considered more optimal. It indicates that our method (i.e., RTPCA) surpasses the others in terms of both accuracy and efficiency.

Contemporary transformer-based methodologies frequently grapple with the limitation of attention mechanisms yielding inadequately diverse and comprehensive information, severely constraining the potential of transformers. In response, certain approaches have endeavored to introduce more holistic information by employing cross-attention mechanisms (Tang et al. 2023; Li et al. 2022; Hu et al. 2022). However, these efforts have remained confined to intra-block contexts, lacking the exploration of multiscale information and inter-block interactions.

To bridge this gap, we put forth the Refined Temporal Pyramidal Compression-and-Amplification (RTPCA) strategy tailored for 3D pose estimation. Our framework is grounded in two primary components: The Temporal Pyramidal Compression-and-Amplification (TPCA) transformer block and a cross-layer feature refinement (XLR) module. TPCA is innovatively engineered to capitalize on temporal pyramidal structures, while the cross-layer feature refinement module, distinct from conventional U-Net (Ronneberger, Fis-

cher, and Brox 2015) and U-Net++ (Zhou et al. 2018) styles, dovetails feature refinement directly into attention operations. This design choice allows later-stage transformer blocks to seamlessly access and assimilate early-stage keys and values, pushing the envelope of attention-driven learning.

As depicted in Figure 1, we conducted a comparison study on the Human3.6M dataset to assess the performance of different methods based on their MPJPE and latency scores. MPJPE was calculated using ground truth 2D key points as input, while latency measured inference speed with a batch size of 1. The value of F represented the number of input frames. It is worth noting that methods that performed closer to the origin of coordinates were considered more optimal. Based on our evaluation, we found that our RTPCA method demonstrated superior accuracy and efficiency compared to the other approaches.

In summary, our contributions are as follows:

- We unveil the RTPCA, a pioneering approach for 3D pose estimation that elegantly reconciles redundancy issues and streamlines feature aggregation. Our TPCA block, built upon a temporal pyramidal compression-and-amplification design, is a groundbreaking solution for curbing redundancies and enhancing robustness against noise in the context of 3D pose estimation.
- Our XLR module is a beacon of innovation. By interweaving feature refinement techniques with a cross-attention strategy, we craft a holistic representation, enabling dynamic interactions across queries, keys, and values from varied layers.
- The potency of RTPCA is validated against recognized benchmarks: Human3.6M, HumanEva-I, and MPI-INF-3DHP. Our model not only stands head and shoulders above its contemporaries in performance but also ensures computational efficiency.

## Related Work

**3D Human Pose Estimation.** 3D Human Pose Estimation (HPE) has gained significant attention in computer vision, focusing on evaluating the 3D joint locations of a single human body from single or multiple views (Wang et al. 2021). Approaches can be primarily categorized as one-stage and two-stage methods. One-stage approaches directly estimate the 3D pose from input images without intermediate 2D pose representation (Li and Chan 2015; Zhou et al. 2016; Sun et al. 2017; Pavlakos et al. 2017; Sun et al. 2018; Ma et al. 2021). Conversely, two-stage methods first detect 2D keypoints from the RGB data and then project these 2D keypoints to a 3D pose (Ci et al. 2019; Liu et al. 2020a; Martinez et al. 2017; Xu and Takano 2021; Zhao et al. 2019). Considering the successful use of 2D keypoint detection in recent two-stage methods, our work adopts this method and primarily focuses on the 2D-to-3D lifting operation.

**Graph Convolution Networks in 3D HPE.** Graph Convolution Networks (GCN) (Kipf and Welling 2016) have been extensively employed in HPE tasks due to their proficiency in encapsulating human skeleton graph information. For example, Wang *et al.* (Wang et al. 2020) introduced a U-shaped GCN architecture and a novel motion loss to ensure

smooth movement, while Hu *et al.* (Hu et al. 2021) proposed a U-shaped conditional directed graph convolutional network (U-CondDGCN). Other studies combined temporal convolution networks (TCN) with GCN to capture both spatial and spectral information (Cai et al. 2019; Le et al. 2021; Cheng et al. 2021; Zhao, Dou, and Feng 2020). However, while these GCN-based approaches achieve impressive results in 3D HPE, they struggle to capture global contextual information across frames efficiently.

**Transformer in 3D HPE.** With the rise of Transformer architectures (Vaswani et al. 2017) and their potent self-attention mechanism, there has been a surge in its applications across a variety of vision tasks (Han et al. 2021; He et al. 2021b; Carion et al. 2020; Dosovitskiy et al. 2021; Liu et al. 2023). For instance, PoseFormer (Zheng et al. 2021) was introduced to model human joint relations within frames as well as temporal correlations across frames using a pure transformer structure. Similarly, other works proposed novel methods combining Transformer and GCN to effectively handle information flow interactions (Zhao et al. 2021), or exploit connections within the network to improve the information exchange via cross-layer fusion (Chen et al. 2023). Nevertheless, these methods typically focus on enhancing individual modules and often overlook the interconnections among them. In contrast, our proposed TPCA method leverages the temporal pyramidal structure and cross-layer refinement mechanism to explore inter and intra-block information within the attention module, thereby bolstering the transformer’s capabilities.

**Inter&Intra Attention Mechanism.** Attention plays a crucial role in transformers, and a more comprehensive exploration of attention information holds the potential to enhance transformer performance. Cross-attention stands as a commonly utilized mechanism for acquiring richer attention patterns. In (Tang et al. 2023), input features are bifurcated into temporal and spatial partitions, followed by concatenation after independent attention learning. (Li et al. 2022) fuses attention from multiple generated hypothesis, while (Hu et al. 2022) integrates features from different views. However, these methods confine fusion within a single block, disregarding inter-block connections, which can lead to significant discrepancies between learned attention in a given block and its subsequent block. To address this, we propose an inter&intra interaction mechanism, merging attention from adjacent stages to heighten model stability and robustness. As for intra-block exploration, numerous efforts have leveraged pyramidal networks to uncover multi-scale information. Inspired by (Wang et al. 2022) and (Yang et al. 2022) which utilize the pyramidal architectures to the network structure and explore multi-scale feature attributes, we devise a pyramidal compression-and-amplification for attention Key & Value, yielding a more comprehensive learning of attention information while simultaneously mitigating noise.

## Methodology

### Framework

The Refined Temporal Pyramidal Compression-and-Amplification (RTPCA) transformer model proposed in this study employs a transformer-based architecture to capture

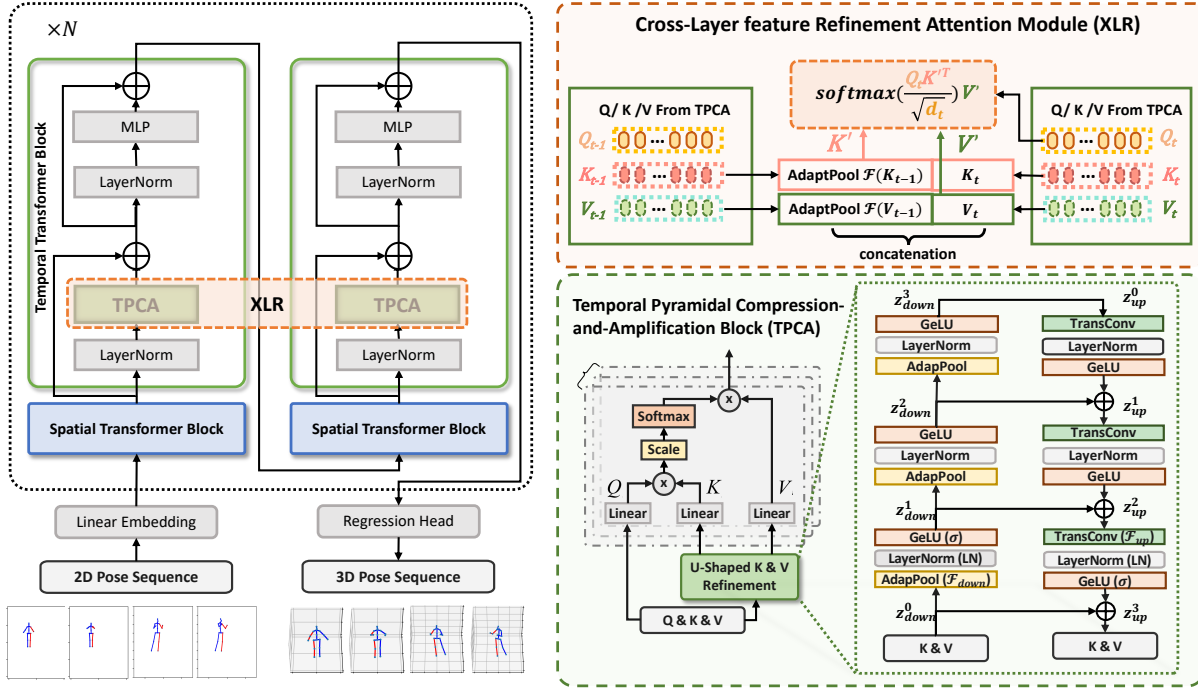


Figure 2: **Framework of the proposed Refined Temporal Pyramidal Compression-and-Amplification (RTPCA).** The network is formed by stacking TPCA blocks to extract multi-scale information in attention. The Cross-Layer Refinement (XLR) module is proposed to fuse inter-block information. The idea is to combine keys and values from both the front and the back for feature aggregation, thereby boosting the capability of the transformer. The input feature dimension equals  $B \times J \times F \times C$ , where  $B$  denotes the batch size,  $F$  is the number of frames,  $J$  is the number of joints and  $C$  represents the channel size.

global patterns among input 2D human poses. The RTPCA model integrates the Spatial-Temporal Encoder (STE) with a Temporal Pyramidal Compression-and-Amplification (TPCA) structure to enhance intra-block temporal modeling and further refines inter-block feature interaction using a cross-layer feature refinement module (XLR). The framework of RTPCA is depicted in Figure 2. The TPCA utilizes key&value refinement to augment the transformer’s capabilities and discover multi-scale attention information. The XLR module is designed to integrate the spatial and semantic information between adjacent temporal encoders in a cross-attention manner, enhancing the model’s capacity to understand and learn inter-block temporal dynamics. The proposed RTPCA structure will be formed by superimposing multiple cross-layer feature refinement modules.

Formally, every frame of the input video is treated as a token in the transformer and represented as  $X_{J,F} \in \mathbb{R}^{B \times J \times F \times 2}$ , where  $B$  denotes the batch size.  $J$  denotes the joints and  $F$  indicates the frames, with 2 representing the 2D coordinates. The input  $X$  is initially projected into a high-dimensional feature space  $Z_{J,F} \in \mathbb{R}^{B \times J \times F \times C}$ , where  $C$  signifies the channel size for each joint. Both temporal and spatial transformers are employed to alternately learn the spatiotemporal information in the input sequence, with the size of the input token reshaped as  $Z_t \in \mathbb{R}^{(B \times J) \times F \times C}$  and  $Z_s \in \mathbb{R}^{(B \times F) \times J \times C}$  respectively.

The transformer encoder takes  $Z_t$  and  $Z_s$  as input, and a

regression head is followed to project the encoder’s output to  $Y_{J,F} \in \mathbb{R}^{B \times J \times F \times 3}$ . The loss function of our proposed model is composed of three main components: Weighted Mean Per Joint Position Error (WMPJPE)  $\mathcal{L}_w$ , Temporal Coherence Loss (TCLoss)  $\mathcal{L}_t$ , and Mean Per Joint Velocity Error (MPJVE)  $\mathcal{L}_m$ . The WMPJPE  $\mathcal{L}_w$  is formulated as  $\mathcal{L}_w = \frac{1}{N} \sum_{i=1}^N \left( W \times \frac{1}{F} \sum_{j=1}^F \|p_{i,j} - g_{i,j}\|_2^2 \right)$ , where  $N$  denotes the  $N$  joints of a human skeleton and  $F$  represents the number of frames in a sequence. The terms  $p_{i,j}$  and  $g_{i,j}$  refer to the predicted and ground truth 3D poses of the  $i$ -th joint at the  $j$ -th frame, respectively.  $W$  is a diagonal matrix consisting of weights for each joint, enabling us to give different importance to different joints. The overall loss function is given by  $\mathcal{L} = \mathcal{L}_w + \lambda_t \mathcal{L}_t + \lambda_m \mathcal{L}_m$ , where  $\lambda_t$  and  $\lambda_m$  are hyper-parameters for balancing the contributions of  $\mathcal{L}_t$  and  $\mathcal{L}_m$ . This design ensures the effective capture and representation of spatial-temporal human pose dynamics, thereby enhancing the performance of 3D human pose estimation.

## Preliminary

The spatial-temporal dynamics of the human pose are typically modeled using two modules: the Spatial Transformer block (ST) and the Temporal Transformer block (TT). These modules are designed to learn the characteristics of human skeleton joints and the trajectories of different joints across frames, respectively.

**Spatial Transformer block.** The Spatial Transformer block (ST) captures the relationship of all joints within the human skeleton in each frame. The joint matrix of each frame is regarded as a spatial attention token  $Z_s \in \mathbb{R}^{(B \times F) \times J \times C}$ . The tokens are then embedded with a spatial position matrix  $E_s \in \mathbb{R}^{(B \times F) \times J \times C}$ , and fed into the transformer’s basic components - multi-head self-attention (MSA) and multi-layer perceptron (MLP), as described in Vaswani et al. (Vaswani et al. 2017). The dimension of the tokens remains unchanged after the feature extraction of ST. This process is formalized as follows:

$$\begin{aligned}\widetilde{\text{ST}}(Z_s) &= Z_s + \text{MSA}(Z_s), \\ \text{ST}(Z_s) &= \widetilde{\text{ST}}(Z_s) + \text{MLP}(\widetilde{\text{ST}}(Z_s)),\end{aligned}\quad (1)$$

In the first ST, the spatial position encoding  $E_s$  is added to  $Z_s$ .  $\text{MSA}(\cdot)$  and  $\text{MLP}(\cdot)$  denote the operation of multi-head self-attention and multi-layer perceptron, respectively.

**Temporal Transformer block.** The Temporal Transformer block (TT), in conjunction with the novel Cross-Layer feature Refinement module (XLR), describes each joint’s trajectory across input frames, mining multi-scale information in attention. It models the different body joint motion trajectories separately, allowing a richer representation of their temporal relationships. The joints are segmented into individual tokens  $Z_t \in \mathbb{R}^{(B \times J) \times F \times C}$  in the temporal direction. Like ST, a time positional encoding  $E_t \in \mathbb{R}^{(B \times J) \times F \times C}$  is added to the input token, which is then fed into TT.

$$\begin{aligned}\widetilde{\text{TT}}(Z_t) &= Z_t + \text{XLR}(Z_{t-1}, Z_t), \\ \text{TT}(Z_t) &= \widetilde{\text{TT}}(Z_t) + \text{MLP}(\widetilde{\text{TT}}(Z_t)),\end{aligned}\quad (2)$$

In the equation above,  $\text{XLR}(\cdot)$  represents the operation of the cross-layer feature refinement module, accepting input tokens from both the previous block  $Z_{t-1}$  and the current block  $Z_t$ , which will be discussed in detail later and will be used to aggregate features in attention and learn more comprehensive information.

### Temporal Pyramidal Compression-and-Amplification Attention Block

In order to achieve a more comprehensive extraction of information from the self-attention layer, we introduce a temporal pyramidal compression-and-amplification attention block (TPCA) to explore the multi-scale information embedded in keys  $K \in \mathbb{R}^{n \times d}$  and values  $V \in \mathbb{R}^{n \times d}$ . The dimension of queries  $Q \in \mathbb{R}^{n \times d}$  is preserved while the keys and values are processed through multiple stages, thereby allowing the attention matrix to learn multi-scale pyramidal information while maintaining the same temporal resolution. As depicted in Figure 2, this block progressively compresses  $K$  and  $V$ , with the sequence length of  $K$  and  $V$  being reduced by a factor of  $r$  at each stage, where  $r$  denotes the sampling ratio. During the compression phase, dimensions are gradually restored through the amplification layers, and residual links are introduced at corresponding phases to facilitate gradient flow.

**TPCA for attention Key & Value.** Pyramidal networks have demonstrated their efficacy in various tasks owing to their

ability to reduce redundancy and capture high-level semantic information while preserving low-level details. To obtain more refined key and value representations, we leverage temporal pyramidal compression-and-amplification network to enhance intra-block exploration. Given the input feature vector  $z \in \mathbb{R}^{n \times d}$  with sequence length  $n$  and channel dimension  $d$ , the TPCA block produces an output feature vector with the same dimensions. The operation of U-shaped temporal attention is represented as  $\text{TPCA}(\cdot)$ . It can be formulated as follows:

$$\begin{aligned}z_{\text{down}}^0 &= z, \quad z_{\text{down}}^{l+1} = \sigma(\text{LN}(\mathcal{F}_{\text{down}}(z_{\text{down}}^l))), \\ z_{\text{up}}^0 &= z_{\text{down}}^m, \quad z_{\text{up}}^{l+1} = \sigma(\text{LN}(\mathcal{F}_{\text{up}}(z_{\text{up}}^l))) + z_{\text{down}}^{m-1-l},\end{aligned}\quad (3)$$

where  $\sigma(\cdot)$  is the activation function,  $\text{LN}(\cdot)$  is the Layer-Norm layer, and  $\mathcal{F}_{\text{down}}$  and  $\mathcal{F}_{\text{up}}$  denote the compression and amplification functions, respectively.  $z_{\text{down}}^l \in \mathbb{R}^{\frac{n}{r^l} \times d}$  and  $z_{\text{up}}^l \in \mathbb{R}^{\frac{n}{r^{m-l}} \times d}$ .  $l \in [0, 1, \dots, m-1]$  is the index of the sampling stage.  $r$  denotes the pooling ratio. The TPCA block first compresses the feature  $z$  for  $m$  stages, then amplifies the feature with a pyramidal connection. The final output  $\text{TPCA}(z) = z_{\text{up}}^m \in \mathbb{R}^{n \times d}$ .

The incorporation of the pyramidal compression-and-amplification attention block for key and value allows for more refined representations to be derived from the data. The compression process enables the distillation of the information, reducing the levels of noise, while the amplification process reinstates the lost information and merges it with higher-level features. The direct use of keys and values may lead to susceptibility to data noise, which can ultimately degrade the model’s performance. Hence, TPCA block provide a robust and efficient method for refining key and value representations, thereby enhancing the overall performance of the model.

### Cross-Layer Refinement Module

Several ConvNet architectures such as HRNet (Sun et al. 2019), EfficientDet (Tan, Pang, and Le 2020), and others, have proven that the aggregation of neighboring layer features is incredibly effective in fusing spatial information and semantics. However, in Transformer architectures, this feature aggregation scheme has not been fully explored. In this study, we propose a novel transformer network that leverages Cross Attention to enhance spatial-temporal semantics. This is accomplished by stacking multiple cross-layer feature refinement (XLR) modules. The structure of a XLR module is demonstrated in Fig.2. Each module is constructed using two neighboring Spatial-Temporal Encoders (STEs), performing feature aggregation between two Temporal Transformer blocks.

Unlike previous ConvNets that employed simple addition and concatenation for feature aggregation, our proposed XLR module utilizes the interaction between queries, keys, and values across two pyramidal compression-and-amplification attention blocks of neighboring STEs. This design effectively and naturally extends feature fusion to the transformer network by leveraging the attention scheme. More formally, the operation of the cross-layer attention, represented by  $\text{XLR}(\cdot)$ ,

Table 1: **Quantitative results on Human3.6M.** The comparisons with state-of-the-art methods on Human3.6M under protocol #1 (top), protocol #2 (middle) using detected 2D poses, and protocol #1 (bottom) using ground truth 2D poses as input are conducted, where methods marked with † are video-based; CPN and GT denote the input 2D poses are estimated by (Chen et al. 2018) and ground truth respectively. The best and the second best results are highlighted in bold and underlined respectively.

Protocol #1 (CPN)	Dir.	Disc	Eat	Greet	Phone	Photo	Pose	Purch.	Sit	SitD.	Smoke	Wait	WalkD.	Walk	WalkT.	Avg.
Pavlakos et al. (CVPR2018)(Pavlakos, Zhou, and Daniilidis 2018)	48.5	54.4	54.4	52.0	59.4	65.3	49.9	52.9	65.8	71.1	56.6	52.9	60.9	44.7	47.8	56.2
Cai et al. (ICCV'2019)(Cai et al. 2019)(†)	44.6	47.4	45.6	48.8	50.8	59.0	47.2	43.9	57.9	61.9	49.7	46.6	51.3	37.1	39.4	48.8
Pavlo et al. (CVPR'2019)(Pavlo et al. 2019)(†)	45.2	46.7	43.3	45.6	48.1	55.1	44.6	44.3	57.3	65.8	47.1	44.0	49.0	32.8	33.9	46.8
Xu et al. (CVPR'2020)(Xu et al. 2020)(†)	37.4	43.5	42.7	42.7	46.6	59.7	41.3	45.1	52.7	60.2	45.8	43.1	47.7	33.7	37.1	45.6
Liu et al. (CVPR'2020)(Liu et al. 2020b)(†)	41.8	44.8	41.1	44.9	47.4	54.1	43.4	42.2	56.2	63.6	45.3	43.5	45.3	31.3	32.2	45.1
Wang et al. (ECCV'2020)(Wang et al. 2020)(†)	41.3	43.9	44.0	42.2	48.0	57.1	42.2	43.2	57.3	61.3	47.0	43.5	47.0	32.6	31.8	45.6
Hu et al. (ACMMM'2021)(Hu et al. 2021)(†)	38.0	43.3	39.1	39.4	45.8	53.6	41.4	41.4	55.5	61.9	44.6	41.9	44.5	31.6	29.4	43.4
Xu et al. (CVPR'2021)(Xu and Takano 2021)	45.2	49.9	47.5	50.9	54.9	66.1	48.5	46.3	59.7	71.5	51.4	48.6	53.9	39.9	44.1	51.9
Zheng et al. (ICCV2021)(Zheng et al. 2021)(†)	41.5	44.8	39.8	42.5	46.5	51.6	42.1	42.0	53.3	60.7	45.5	43.3	46.1	31.8	32.2	44.3
Li et al. (CVPR'2022)(Li et al. 2022)(†)	39.2	43.1	40.1	40.9	44.9	51.2	40.6	41.3	53.5	60.3	43.7	41.1	43.8	29.8	30.6	43.0
Zhang et al. (CVPR'2022)(Zhang et al. 2022)(†)	<u>37.6</u>	<u>40.9</u>	<u>37.3</u>	39.7	<u>42.3</u>	<u>49.9</u>	<u>40.1</u>	<u>39.8</u>	<u>51.7</u>	<u>55.0</u>	<u>42.1</u>	<u>39.8</u>	<u>41.0</u>	<u>27.9</u>	<u>27.9</u>	<u>40.9</u>
Ours(†)	<b>36.2</b>	<b>38.9</b>	<b>36.7</b>	<b>37.3</b>	<b>41.7</b>	<b>48.3</b>	<b>36.6</b>	<b>39.5</b>	<b>51.3</b>	<u>57.2</u>	<b>41.4</b>	<b>39.5</b>	<b>40.6</b>	<b>27.3</b>	<b>27.3</b>	<b>40.1</b>
Protocol #2 (CPN)	Dir.	Disc	Eat	Greet	Phone	Photo	Pose	Purch.	Sit	SitD.	Smoke	Wait	WalkD.	Walk	WalkT.	Avg.
Cai et al. (ICCV'2019)(Cai et al. 2019)(†)	35.7	37.8	36.9	40.7	39.6	45.2	37.4	34.5	46.9	50.1	40.5	36.1	41.0	29.6	33.2	39.0
Pavlo et al. (CVPR'2019)(Pavlo et al. 2019)(†)	34.1	36.1	34.4	37.2	36.4	42.2	34.4	33.6	45.0	52.5	37.4	33.8	37.8	25.6	27.3	36.5
Xu et al. (CVPR'2020)(Xu et al. 2020)(†)	31.0	34.8	34.7	34.4	36.2	43.9	31.6	33.5	42.3	49.0	37.1	33.0	39.1	26.9	31.9	36.2
Liu et al. (CVPR'2020)(Liu et al. 2020b)(†)	32.3	35.2	33.3	35.8	35.9	41.5	33.2	32.7	44.6	50.9	37.0	32.4	37.0	25.2	27.2	35.6
Wang et al. (ECCV'2020)(Wang et al. 2020)(†)	32.9	35.2	35.6	34.4	36.4	42.7	31.2	32.5	45.6	50.2	37.3	32.8	36.3	26.0	23.9	35.5
Hu et al. (ACMMM'2021)(Hu et al. 2021)(†)	<u>29.8</u>	34.4	31.9	<u>31.5</u>	35.1	40.0	<u>30.3</u>	30.8	42.6	49.0	35.9	31.8	35.0	25.7	23.6	33.8
Zhang et al. (CVPR2022)(Zhang et al. 2022)(†)	30.8	<u>33.1</u>	<b>30.3</b>	31.8	<u>33.1</u>	<u>39.1</u>	31.1	<b>30.5</b>	<u>42.5</u>	<b>44.5</b>	<u>34.0</u>	<u>30.8</u>	<u>32.7</u>	<u>22.1</u>	<u>22.9</u>	<u>32.6</u>
Ours(†)	<b>29.6</b>	<b>32.0</b>	<u>30.7</u>	<b>30.5</b>	<b>32.3</b>	<b>37.2</b>	<b>28.6</b>	<u>30.6</u>	<b>41.3</b>	<u>47.2</u>	<b>33.2</b>	<b>30.3</b>	<b>31.7</b>	<b>21.1</b>	<b>22.2</b>	<b>32.0</b>
Protocol #1 (GT)	Dir.	Disc	Eat	Greet	Phone	Photo	Pose	Purch.	Sit	SitD.	Smoke	Wait	WalkD.	Walk	WalkT.	Avg.
Pavlo et al. (CVPR'2019)(Pavlo et al. 2019)(†)	35.2	40.2	32.7	35.7	38.2	45.5	40.6	36.1	48.8	47.3	37.8	39.7	38.7	27.8	29.5	37.8
Zeng et al. (ECCV'2020)(Zeng et al. 2020)(†)	34.8	32.1	28.5	30.7	31.4	36.9	35.6	30.5	38.9	40.5	32.5	31.0	29.9	22.5	24.5	32.0
Zheng et al. (ICCV2021)(Zheng et al. 2021)(†)	30.0	33.6	29.9	31.0	30.2	33.3	34.8	31.4	37.8	38.6	31.7	31.5	29.0	23.3	23.1	31.3
Li et al. (CVPR'2022)(Li et al. 2022)(†)	27.7	32.1	29.1	28.9	30.0	33.9	33.0	31.2	37.0	39.3	30.0	31.0	29.4	22.2	23.0	30.5
Zhang et al. (CVPR2022)(Zhang et al. 2022)(†)	<u>21.6</u>	<u>22.0</u>	<u>20.4</u>	<u>21.0</u>	<u>20.8</u>	<u>24.3</u>	<u>24.7</u>	<u>21.9</u>	<u>26.9</u>	<b>24.9</b>	<u>21.2</u>	<u>21.5</u>	<u>20.8</u>	<u>14.7</u>	<u>15.7</u>	<u>21.6</u>
Ours(†)	<b>18.5</b>	<b>19.5</b>	<b>18.5</b>	<b>19.1</b>	<b>19.6</b>	<b>22.3</b>	<b>21.6</b>	<b>19.1</b>	<b>26.2</b>	<u>25.3</u>	<b>19.1</b>	<b>19.3</b>	<b>18.5</b>	<b>12.5</b>	<b>12.8</b>	<b>19.5</b>

can be formulated as,

$$\begin{aligned}
\text{XLR} &= \text{Attn}(Z_{t-1}, Z_t) \\
&= \text{Attn}(Q_t, K', V'), \\
&= \text{Softmax}\left(\frac{Q_t K'^T}{\sqrt{d}}\right) V', \\
K' &= \text{Concat}(K_t, \mathcal{F}(K_{t-1})), \\
V' &= \text{Concat}(V_t, \mathcal{F}(V_{t-1})),
\end{aligned} \tag{4}$$

where  $Z_{t-1}$  and  $Z_t$  are the latent features of the previous and current block respectively and  $Z_t$  can be projected into query, key, and value through different weight matrices.  $Q_t$ ,  $K_t$ , and  $V_t$  are the query, key, and value from the second TT.  $K_{t-1}$  and  $V_{t-1}$  are the keys and values from the first TT.  $K'$  and  $V'$  are derived from the cross-layer attention using equation 4, where  $\text{Concat}$  denotes the concatenation operation,  $\mathcal{F}$  is the adaptive pooling operated on  $K_{t-1}$  and  $V_{t-1}$  from the first TT. Both  $K_t$ ,  $V_t$  and  $K_{t-1}$ ,  $V_{t-1}$  are processed after pyramidal compression-and-amplification attention block. By concatenating the refined key and value using TPCA block from the second TT and the pooled refined key and value from the first TT, multi-scale information and more comprehensive details can be obtained.

## Experiment

### Datasets and Metric

For our experimentation, we used three key 3D pose estimation benchmark datasets: Human3.6M (Ionescu et al. 2014), HumanEva-I (Sigal, Balan, and Black 2010), and MPI-INF-3DHP (Mehta et al. 2017a). Human3.6M is widely considered the industry standard for 3D pose evaluation, boast-

ing 3.6 million video frames captured from four synchronized cameras at 50 Hz, each positioned differently. The dataset encompasses 11 subjects executing 15 different actions. HumanEva-I, while smaller in comparison with fewer subjects and actions, is still a robust dataset for 3D pose estimation. Following the practice of (Pavlo et al. 2019) and (Lee, Lee, and Lee 2018), we utilized all actions (Walk, Jog, Box) from subjects  $S_1$ ,  $S_2$ , and  $S_3$  for our training. The MPI-INF-3DHP contains both indoor and outdoor environmental datasets, involving more diverse motions than Human3.6M and HumanEva-I.

To maintain comparability with previous work (Hu et al. 2021; Cai et al. 2019; Zhang et al. 2022; Zhao, Wang, and Tian 2022), we adopted the Mean Per Joint Position Error (MPJPE) for Human3.6M and HumanEva-I, MPJPE, Percentage of Correct Keypoints(PCK) with the threshold of 150mm, and Area Under Curve (AUC) for a range of PCK thresholds for MPI-INF-3DHP as our evaluation metric.

### Implementation Details

We implemented the proposed RTPCA using the PyTorch framework<sup>1</sup>, and our experiments were performed on two NVIDIA TITAN V100 GPUs. For performance analysis, we utilized 2D keypoints derived from a 2D pose detector (Chen et al. 2018), as well as from 2D ground truth. The model was optimized using the Adam optimizer (Kingma and Ba 2014), and we established the batch size, dropout rate, and activation function at 1024, 0.1, and GELU, respectively. Following the example set by (Zhang et al. 2022), we designated the input sequence length to 243 for Human3.6M and 27

<sup>1</sup><https://pytorch.org>

Table 2: **Quantitative results on HumanEva-I dataset under protocol #1.** The best result is highlighted in bold.

Protocol #1	Walk			Jog			Avg.
p-LSTMs (Lee, Lee, and Lee 2018)	18.6	19.9	30.5	25.7	16.8	17.7	30.3
PoseFormer (Zheng et al. 2021)	16.3	11.0	47.1	25.0	15.2	15.1	21.6
MixSTE (Zhang et al. 2022)	20.3	22.4	34.8	27.3	32.1	34.3	28.5
Ours	18.8	17.8	21.2	18.5	21.2	21.3	<b>19.1</b>

for HumanEva-I and MPI-INF-3DHP. The weights assigned in WMPJPE were differentiated based on joint groups, attributing 1.0 to the torso, 1.5 to the head, 2.5 to the middle limb, and 4.0 to the terminal limb. The  $\lambda_t$  and  $\lambda_m$  were referred to (Zhang et al. 2022). In order to prevent overlapping frames between sequences, we applied a stride data sampling strategy, where the interval matches the input length.

### Comparison with the State-of-the-Arts

**Human3.6M Results** In order to gauge the performance of our proposed approach, we compared it with the current state-of-the-art methods using the Human3.6M dataset (Ionescu et al. 2014). For accuracy, we’ve referenced the performance numbers reported in the original papers of these competing methods. A comparison of our approach with both graph ConvNet-based and Transformer-based methods is summarized in Table 1.

The current state-of-the-art method, MixSTE (Zhang et al. 2022), achieves a 21.6mm MPJPE using an input of 243 frames derived from the 2D ground truth pose. Our method surpasses this result, achieving a 19.5mm MPJPE and thereby outperforming the state-of-the-art by 2.7mm, while utilizing nearly the same number of parameters as MixSTE.

The top and middle sections of Table 1 illustrate the MPJPE achieved using detected 2D poses, with CPN (Chen et al. 2018) adopted as the 2D pose detector. Despite the change in input, our method still yields the best result, achieving an MPJPE of 40.1mm under protocol #1, surpassing the state-of-the-art by 0.8mm and securing the best results across all actions with the exception of the *Greet* action. Under protocol #2, which uses P-MPJPE as the evaluation metric, our method improves by 0.6mm over the second-best method.

Table 1 also lists the performance of both video-based and non-video-based approaches, illustrating that video-based methods generally outperform their non-video counterparts, owing to the integration of temporal information. In all settings, our method outperforms other methods, demonstrating its robustness and superiority.

**HumanEva-I Results** To assess the generalization ability of our proposed method, we compared its performance with state-of-the-art methods using the HumanEva-I benchmark. As shown in Table 2, the MPJPE results on HumanEva-I validate our method’s effectiveness and transferability, mirroring the trend observed on the Human3.6M dataset. Once again, our proposed model achieves state-of-the-art performance.

**MPI-INF-3DHP Results** Table 3 shows a quantitative comparison of different state-of-the-art methods for 3D hu-

Table 3: **Quantitative comparisons with state-of-the-art methods on MPI-INF-3DHP with three metrics.** Best in bold, second best best underlined.

Method	PCK[↑]	AUC[↑]	MPJPE[↓]
VNect (Mehta et al. 2017b)	79.4	41.6	-
TrajectoryPose3D (Lin and Lee 2019)	83.6	51.4	79.8
UGCN (Wang et al. 2020)	86.9	62.1	68.1
U-CondDGCN (Hu et al. 2021)	97.9	<u>69.5</u>	<u>42.5</u>
PoseAug (Gong, Zhang, and Feng 2021)	88.6	57.3	73.0
MixSTE (Zhang et al. 2022)	<u>94.4</u>	66.5	54.9
Ours	<b>98.8</b>	<b>74.2</b>	<b>40.5</b>

Table 4: **Ablation study for each component used in our method. TPCA block and XLR module are explained in the 3rd and 4th parts, respectively.** The evaluation is conducted on Human3.6M with MPJPE(mm), Parameters(M), and FLOPs(G).

Method	STE	TPCA	XLR	MPJPE[↓]	Params	FLOPs
Baseline	✓	✗	✗	21.7	33.78	139.0
	✓	✓	✗	20.0	33.84	139.4
Ours	✓	✓	✓	<b>19.5</b>	33.91	139.4

man pose estimation on MPI-INF-3DHP dataset under PCK, AUC, and MPJPE metrics. The proposed method achieves the best performance across all metrics, outperforming other approaches. Considering that the MPI-INF-3DHP dataset encompasses diverse indoor and outdoor scenarios, the superior performance of our method highlights its adaptability to complex environments. The ability to achieve better results across all metrics suggests that our method can effectively handle noise and variations present in real-world settings.

### Ablation Study

In order to thoroughly verify the effectiveness of each element and design strategy incorporated in our proposed model, we conducted extensive ablation experiments using the Human3.6M dataset under protocol 1 and 2D ground truth human pose as input.

**Impact of Model Components** We evaluated our model’s components by sequentially incorporating them and measur-

Table 5: **Ablation study for the noisy input and accelation error loss.** Acceleration error, MPJPE using noisy ground truth 2D keypoints as input, and MPJPE using ground truth 2D keypoints as input are showcased in this table. The best result is highlighted in bold.

Method	Accel[↓]	MPJPE(noisy input)[↓]	MPJPE[↓]
STE	22.4	30.8	21.7
STE+TPCA	10.7	23.3	20.0
STE+XLR	8.5	25.7	20.9
RTPCA	<b>7.3</b>	<b>20.8</b>	<b>19.5</b>

Table 6: **Ablation study for the structure of TPCA.** Different compression and amplification methods are analyzed in this table. Compression methods include adaptively pooling and convolution while amplification methods include linear interpolation and transpose convolution.

<i>Compression</i>		<i>Amplification</i>		MPJPE[↓]
Pool	Conv	Linear	Trans-Conv	
✓				20.9
	✓			22.1
✓	✓			20.6
✓			✓	<b>20.0</b>
✓	✓	✓		20.1
✓	✓		✓	20.9

ing their impact on Mean Per Joint Position Error (MPJPE), as shown in Table 4. Starting with the baseline Spatial-Temporal Transformer (STE) akin to the state-of-the-art method (Zhang et al. 2022), we maintained parameter parity for a fair MPJPE comparison. Integration of the TPCA block, led to a notable MPJPE reduction of 1.7 units, showcasing the value of extracted multiscale feature information. Subsequent application of the XLR module further improved pose estimation outcomes without substantial parameter or FLOP increments.

To assess noise reduction and stability enhancement, we introduced Gaussian noise to ground truth 2D human keypoints. The results in Table 5 underscore the minimal susceptibility of our approach to perturbations, with the TPCA module significantly contributing to the model resilience, complemented by the influence of the XLR module. For gauging stability, the acceleration error (Accel), measuring the difference between the predicted and ground truth 3D acceleration for each keypoint in  $mm/s^2$  is reported for comparison. Notably, the TPCA component exhibited the lowest Accel value, signifying that our methodology enhances stability, with substantial influence from the XLR module.

**Impact of TPCA Block** The TPCA block in our method is designed to effectively extract multiscale feature information from the attention matrix. We utilized a temporal pyramidal compression-and-amplification for  $K$  and  $V$  to implement the feature extraction. To compare with other structures, we considered various compression and amplification strategies. For compression, we initially considered two widely used methods, adaptively pooling and convolution, for  $K$  and  $V$ , respectively. Subsequently, we included an amplification stage to create the pyramidal structure. As shown in Table 6, the pyramidal compression-amplification structure outperforms the compression strategy alone, as evidenced by the better results achieved in the last three rows compared to the first three rows. We tested three different compression strategies and found that the combination of adaptive pooling and transpose convolution achieved the best performance, resulting in an MPJPE of 20.0, which was used in our other experiments.

Table 7: **Ablation study for the connections of XLR.** Cross-connection and residual cross-connection are conducted in this experiment to explore the performance of different structures of cross-layer refinement modules.

Method	MPJPE[↓]
TPCA	20.0
TPCA, Pyramidal XLR (Pyramidal $Q$ )	21.2
TPCA, Pyramidal XLR (Constant $Q$ )	19.9
TPCA, Residual XLR (Constant $Q$ )	<b>19.5</b>

**Impact of Cross-Layer Connections** The Cross-Layer feature Refinement (XLR) Module in our model features a contiguous connection strategy. To evaluate the impact of this strategy, we conducted various ablation studies, summarized in Table 7. We started by applying the TPCA alone to the STE as a baseline, yielding an MPJPE of 20.0. The pyramidal XLR represents the connections between earlier and later TPCAs at the front and back ends, not immediately adjacent to each other. Pyramidal  $Q$  denotes the inclusion of an extra-temporal linear layer in the Temporal Transformer (TT) to alter the output dimension of the frames, thereby creating a pyramidal structure of frame dimensions throughout the model. The results (2nd row in Table 7) indicate that as the dimension of  $Q$  decreases, there is information loss and the model’s effectiveness decreases. The combination of TPCA and pyramidal connection results in a slight improvement over the baseline (3rd row in Table 7). The adjacent connection strategy is found to be most effective after experimenting with different shapes of cross-layer connections (last row in Table 7). This strategy is adopted in our model due to its proven efficiency.

## Visualization and Qualitative Results

The visual comparison in Figure 3 vividly showcases the efficacy of our proposed RTPCA compared to the prevailing state-of-the-art (SOTA) method, MixSTE, as well as ground truth. This visualization elucidates our model’s capability to generate highly accurate human poses, thus affirming its proficiency in handling a diverse spectrum of actions. Notably, our approach demonstrates exceptional performance even in challenging scenarios characterized by occlusion, as evidenced by the illustrative cases presented in the first and second rows of the figure. The comprehensive visual evaluation underscores the robustness and reliability of our model, which can accurately capture complex human pose variations across different activities.

## Conclusion

In this paper, we introduce the RTPCA transformer, a cutting-edge framework for enhancing temporal modeling in 3D Human Pose Estimation. Our framework employs a pyramidal compression-and-amplification structure to boost the intra-block temporal dimension while incorporating a cross-layer attention mechanism to improve inter-block feature interaction. Through the TPCA block, we use a temporal pyramid paradigm to extract spatial semantics from motion



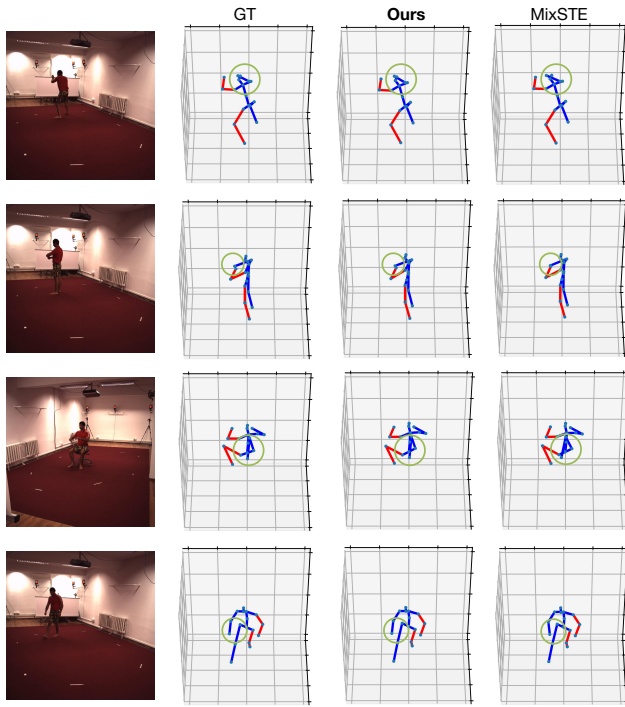


Figure 3: **Comparison of 3D estimated human pose generated by different methods.** The 3D reconstruction visualization results using our proposed method, state-of-the-art method MixSTE, ground truth, and the corresponding video frame in the Human3.6M dataset are shown in this figure. Our method shows higher accuracy and robustness in handling various actions and occlusion scenarios.

sequences while representing keys and values. These blocks are connected via the XLR module, which facilitates dynamic interactions among queries, keys, and values, combining early-stage information with current flows to achieve superior accuracy and stability compared to other transformer-based baselines. Extensive experiments demonstrate that our method has achieved impressive results in 3D human pose estimation, exhibiting robustness and stability in the presence of disturbances.

## References

Cai, Y.; Ge, L.; Liu, J.; Cai, J.; Cham, T.-J.; Yuan, J.; and Thalmann, N. M. 2019. Exploiting Spatial-Temporal Relationships for 3D Pose Estimation via Graph Convolutional Networks. In *Proceedings of the IEEE/CVF international conference on computer vision*, 2272–2281. Seoul, Korea (South): IEEE. ISBN 978-1-72814-803-8.

Carion, N.; Massa, F.; Synnaeve, G.; Usunier, N.; Kirillov, A.; and Zagoruyko, S. 2020. End-to-end object detection with transformers. In *Computer Vision—ECCV 2020: 16th European Conference, Glasgow, UK, August 23–28, 2020, Proceedings, Part I 16*, 213–229. Springer.

Chen, C.-F.; Fan, Q.; and Panda, R. 2021. CrossViT: Cross-

Attention Multi-Scale Vision Transformer for Image Classification. *arXiv:2103.14899*.

Chen, H.; He, J.; Xiang, W.; Liu, W.; Cheng, Z.; Liu, H.; Luo, B.; Geng, Y.; and Xie, X. 2023. HDEformer: High-order Directed Transformer for 3D Human Pose Estimation. *CoRR*, abs/2302.01825.

Chen, Y.; Wang, Z.; Peng, Y.; Zhang, Z.; Yu, G.; and Sun, J. 2018. Cascaded Pyramid Network for Multi-Person Pose Estimation.

Cheng, Y.; Wang, B.; Yang, B.; and Tan, R. T. 2021. Graph and temporal convolutional networks for 3d multi-person pose estimation in monocular videos. In *Proceedings of the AAAI Conference on Artificial Intelligence*, volume 35, 1157–1165.

Cheng, Z.-Q.; Dai, Q.; Li, S.; Mitamura, T.; and Hauptmann, A. 2022. Gsrformer: Grounded situation recognition transformer with alternate semantic attention refinement. In *Proceedings of the 30th ACM International Conference on Multimedia*, 3272–3281.

Ci, H.; Wang, C.; Ma, X.; and Wang, Y. 2019. Optimizing network structure for 3d human pose estimation. In *Proceedings of the IEEE/CVF international conference on computer vision*, 2262–2271.

Dosovitskiy, A.; Beyer, L.; Kolesnikov, A.; Weissenborn, D.; Zhai, X.; Unterthiner, T.; Dehghani, M.; Minderer, M.; Heigold, G.; Gelly, S.; Uszkoreit, J.; and Houlsby, N. 2021. An Image is Worth 16x16 Words: Transformers for Image Recognition at Scale. In *International Conference on Learning Representations (ICLR)*.

Gong, K.; Zhang, J.; and Feng, J. 2021. Poseaug: A differentiable pose augmentation framework for 3d human pose estimation. In *Proceedings of the IEEE/CVF conference on computer vision and pattern recognition*, 8575–8584.

Han, K.; Xiao, A.; Wu, E.; Guo, J.; Xu, C.; and Wang, Y. 2021. Transformer in transformer. *Advances in Neural Information Processing Systems*, 34: 15908–15919.

Hassanin, M.; Khamiss, A.; Bennamoun, M.; Boussaid, F.; and Radwan, I. 2022. CrossFormer: Cross Spatio-Temporal Transformer for 3D Human Pose Estimation. *arXiv preprint arXiv:2203.13387*.

Hauptmann, A.; Yu, L.; Liu, W.; Qian, Y.; Cheng, Z.; Gui, L.; et al. 2023. Robust Automatic Detection of Traffic Activity.

He, J.-Y.; Wu, X.; Cheng, Z.-Q.; Yuan, Z.; and Jiang, Y.-G. 2021a. DB-LSTM: Densely-connected Bi-directional LSTM for human action recognition. *Neurocomputing*, 444: 319–331.

He, S.; Luo, H.; Wang, P.; Wang, F.; Li, H.; and Jiang, W. 2021b. Transreid: Transformer-based object re-identification. In *Proceedings of the IEEE/CVF international conference on computer vision*, 15013–15022.

Hu, B.; Zhu, C.; Ai, X.; and Agrawal, S. K. 2022. Acnet: Attention cube regression network for multi-view real-time 3d human pose estimation in telemedicine. *arXiv preprint arXiv:2210.05130*.

Hu, W.; Zhang, C.; Zhan, F.; Zhang, L.; and Wong, T.-T. 2021. Conditional directed graph convolution for 3d human pose



- estimation. In *Proceedings of the 29th ACM International Conference on Multimedia*, 602–611.
- Ionescu, C.; Papava, D.; Olaru, V.; and Sminchisescu, C. 2014. Human3.6M: Large Scale Datasets and Predictive Methods for 3D Human Sensing in Natural Environments. *IEEE Trans. Pattern Anal. Mach. Intell.*, 36(7): 1325–1339.
- Kingma, D. P.; and Ba, J. 2014. Adam: A method for stochastic optimization. *arXiv preprint arXiv:1412.6980*.
- Kipf, T. N.; and Welling, M. 2016. Semi-supervised classification with graph convolutional networks. *arXiv preprint arXiv:1609.02907*.
- Le, V.-T.; Tran, T.-H.; Hoang, V.-N.; Le, V.-H.; Le, T.-L.; and Vu, H. 2021. Sst-gcn: Structure aware spatial-temporal gcn for 3d hand pose estimation. In *2021 13th International Conference on Knowledge and Systems Engineering (KSE)*, 1–6. IEEE.
- Lee, K.; Lee, I.; and Lee, S. 2018. Propagating lstm: 3d pose estimation based on joint interdependency. In *Proceedings of the European conference on computer vision (ECCV)*, 119–135.
- Li, S.; and Chan, A. B. 2015. 3d human pose estimation from monocular images with deep convolutional neural network. In *Computer Vision—ACCV 2014: 12th Asian Conference on Computer Vision, Singapore, Singapore, November 1-5, 2014, Revised Selected Papers, Part II 12*, 332–347. Springer.
- Li, W.; Liu, H.; Tang, H.; Wang, P.; and Van Gool, L. 2022. Mhformer: Multi-hypothesis transformer for 3d human pose estimation. In *Proceedings of the IEEE/CVF Conference on Computer Vision and Pattern Recognition*, 13147–13156.
- Lin, J.; and Lee, G. H. 2019. Trajectory Space Factorization for Deep Video-Based 3D Human Pose Estimation. *arXiv:1908.08289*.
- Liu, H.; He, J.-Y.; Cheng, Z.-Q.; Xiang, W.; Yang, Q.; Chai, W.; Wang, G.; Bao, X.; Luo, B.; Geng, Y.; et al. 2023. PoSynDA: Multi-Hypothesis Pose Synthesis Domain Adaptation for Robust 3D Human Pose Estimation. *arXiv preprint arXiv:2308.09678*.
- Liu, K.; Ding, R.; Zou, Z.; Wang, L.; and Tang, W. 2020a. A comprehensive study of weight sharing in graph networks for 3d human pose estimation. In *Computer Vision—ECCV 2020: 16th European Conference, Glasgow, UK, August 23–28, 2020, Proceedings, Part X 16*, 318–334. Springer.
- Liu, R.; Shen, J.; Wang, H.; Chen, C.; Cheung, S.-c.; and Asari, V. 2020b. Attention Mechanism Exploits Temporal Contexts: Real-Time 3D Human Pose Reconstruction. 5064–5073.
- Ma, X.; Su, J.; Wang, C.; Ci, H.; and Wang, Y. 2021. Context modeling in 3d human pose estimation: A unified perspective. In *Proceedings of the IEEE/CVF conference on computer vision and pattern recognition*, 6238–6247.
- Martinez, J.; Hossain, R.; Romero, J.; and Little, J. J. 2017. A simple yet effective baseline for 3d human pose estimation. In *Proceedings of the IEEE international conference on computer vision*, 2640–2649.
- Mehta, D.; Rhodin, H.; Casas, D.; Fua, P.; Sotnychenko, O.; Xu, W.; and Theobalt, C. 2017a. Monocular 3d human pose estimation in the wild using improved cnn supervision. In *2017 international conference on 3D vision (3DV)*, 506–516. IEEE.
- Mehta, D.; Sridhar, S.; Sotnychenko, O.; Rhodin, H.; Shafiei, M.; Seidel, H.-P.; Xu, W.; Casas, D.; and Theobalt, C. 2017b. VNect: Real-time 3D Human Pose Estimation with a Single RGB Camera. *ACM Transactions on Graphics*, 36(4): 1–14.
- Pavlakos, G.; Zhou, X.; and Daniilidis, K. 2018. Ordinal depth supervision for 3d human pose estimation. In *Proceedings of the IEEE conference on computer vision and pattern recognition*, 7307–7316.
- Pavlakos, G.; Zhou, X.; Derpanis, K. G.; and Daniilidis, K. 2017. Coarse-to-fine volumetric prediction for single-image 3D human pose. In *Proceedings of the IEEE conference on computer vision and pattern recognition*, 7025–7034.
- Pavlo, D.; Feichtenhofer, C.; Grangier, D.; and Auli, M. 2019. 3D Human Pose Estimation in Video with Temporal Convolutions and Semi-Supervised Training. *arXiv*.
- Ronneberger, O.; Fischer, P.; and Brox, T. 2015. U-net: Convolutional networks for biomedical image segmentation. In *Medical Image Computing and Computer-Assisted Intervention—MICCAI 2015: 18th International Conference, Munich, Germany, October 5-9, 2015, Proceedings, Part III 18*, 234–241. Springer.
- Sigal, L.; Balan, A. O.; and Black, M. J. 2010. Humaneva: Synchronized video and motion capture dataset and baseline algorithm for evaluation of articulated human motion. *International journal of computer vision*, 87(1-2): 4–27.
- Sun, K.; Xiao, B.; Liu, D.; and Wang, J. 2019. Deep high-resolution representation learning for human pose estimation. In *Proceedings of the IEEE/CVF conference on computer vision and pattern recognition*, 5693–5703.
- Sun, X.; Shang, J.; Liang, S.; and Wei, Y. 2017. Compositional human pose regression. In *Proceedings of the IEEE international conference on computer vision*, 2602–2611.
- Sun, X.; Xiao, B.; Wei, F.; Liang, S.; and Wei, Y. 2018. Integral human pose regression. In *Proceedings of the European conference on computer vision (ECCV)*, 529–545.
- Tan, M.; Pang, R.; and Le, Q. V. 2020. Efficientdet: Scalable and efficient object detection. In *Proceedings of the IEEE/CVF conference on computer vision and pattern recognition*, 10781–10790.
- Tang, Z.; Qiu, Z.; Hao, Y.; Hong, R.; and Yao, T. 2023. 3D Human Pose Estimation With Spatio-Temporal Criss-Cross Attention. In *Proceedings of the IEEE/CVF Conference on Computer Vision and Pattern Recognition*, 4790–4799.
- Tu, S.; Dai, Q.; Wu, Z.; Cheng, Z.-Q.; Hu, H.; and Jiang, Y.-G. 2023. Implicit temporal modeling with learnable alignment for video recognition. *arXiv preprint arXiv:2304.10465*.
- Vaswani, A.; Shazeer, N.; Parmar, N.; Uszkoreit, J.; Jones, L.; Gomez, A. N.; Kaiser, Ł.; and Polosukhin, I. 2017. Attention is all you need. *Advances in neural information processing systems*, 30.
- Wang, J.; Tan, S.; Zhen, X.; Xu, S.; Zheng, F.; He, Z.; and Shao, L. 2021. Deep 3D human pose estimation: A review. *Computer Vision and Image Understanding*, 210: 103225.

- Wang, J.; Yan, S.; Xiong, Y.; and Lin, D. 2020. Motion guided 3d pose estimation from videos. In *Computer Vision—ECCV 2020: 16th European Conference, Glasgow, UK, August 23–28, 2020, Proceedings, Part XIII 16*, 764–780. Springer.
- Wang, Y.-J.; Luo, Y.-M.; Bai, G.-H.; and Guo, J.-M. 2022. UformPose: A U-Shaped Hierarchical Multi-Scale Keypoint-Aware Framework for Human Pose Estimation. *IEEE Transactions on Circuits and Systems for Video Technology*, 33(4): 1697–1709.
- Xu, J.; Yu, Z.; Ni, B.; Yang, J.; Yang, X.; and Zhang, W. 2020. Deep Kinematics Analysis for Monocular 3D Human Pose Estimation. 899–908.
- Xu, T.; and Takano, W. 2021. Graph stacked hourglass networks for 3d human pose estimation. In *Proceedings of the IEEE/CVF conference on computer vision and pattern recognition*, 16105–16114.
- Yang, H.; Guo, L.; Zhang, Y.; and Wu, X. 2022. U-shaped spatial-temporal transformer network for 3D human pose estimation. *Machine Vision and Applications*, 33(6): 82.
- Zeng, A.; Sun, X.; Huang, F.; Liu, M.; Xu, Q.; and Lin, S. 2020. Srnet: Improving generalization in 3d human pose estimation with a split-and-recombine approach. In *Computer Vision—ECCV 2020: 16th European Conference, Glasgow, UK, August 23–28, 2020, Proceedings, Part XIV 16*, 507–523. Springer.
- Zhang, J.; Tu, Z.; Yang, J.; Chen, Y.; and Yuan, J. 2022. MixSTE: Seq2seq Mixed Spatio-Temporal Encoder for 3D Human Pose Estimation in Video. In *IEEE Conference on Computer Vision and Pattern Recognition (CVPR)*, 13222–13232.
- Zhao, L.; Peng, X.; Tian, Y.; Kapadia, M.; and Metaxas, D. N. 2019. Semantic graph convolutional networks for 3d human pose regression. In *Proceedings of the IEEE/CVF conference on computer vision and pattern recognition*, 3425–3435.
- Zhao, W.; Tian, Y.; Ye, Q.; Jiao, J.; and Wang, W. 2021. Graformer: Graph convolution transformer for 3d pose estimation. *arXiv preprint arXiv:2109.08364*.
- Zhao, W.; Wang, W.; and Tian, Y. 2022. GraFormer: Graph-Oriented Transformer for 3D Pose Estimation. 20438–20447.
- Zhao, Y.; Dou, Y.; and Feng, J. 2020. Temporally refined graph u-nets for human shape and pose estimation from monocular videos. *IEEE Signal Processing Letters*, 27: 1949–1953.
- Zheng, C.; Zhu, S.; Mendieta, M.; Yang, T.; Chen, C.; and Ding, Z. 2021. 3D Human Pose Estimation with Spatial and Temporal Transformers. In *Proceedings of the IEEE/CVF International Conference on Computer Vision*, 11636–11645. Montreal, QC, Canada: IEEE. ISBN 978-1-66542-812-5.
- Zhou, X.; Sun, X.; Zhang, W.; Liang, S.; and Wei, Y. 2016. Deep kinematic pose regression. In *Computer Vision—ECCV 2016 Workshops: Amsterdam, The Netherlands, October 8–10 and 15–16, 2016, Proceedings, Part III 14*, 186–201. Springer.
- Zhou, Y.; Cheng, Z.-Q.; He, J.-Y.; Luo, B.; Geng, Y.; Xie, X.; and Keuper, M. 2023. Overcoming Topology Agnosticism: Enhancing Skeleton-Based Action Recognition through Redefined Skeletal Topology Awareness. *arXiv preprint arXiv:2305.11468*.
- Zhou, Y.; Cheng, Z.-Q.; Li, C.; Geng, Y.; Xie, X.; and Keuper, M. 2022. Hypergraph transformer for skeleton-based action recognition. *arXiv preprint arXiv:2211.09590*.
- Zhou, Z.; Rahman Siddiquee, M. M.; Tajbakhsh, N.; and Liang, J. 2018. Unet++: A nested u-net architecture for medical image segmentation. In *Deep Learning in Medical Image Analysis and Multimodal Learning for Clinical Decision Support: 4th International Workshop, DLMIA 2018, and 8th International Workshop, ML-CDS 2018, Held in Conjunction with MICCAI 2018, Granada, Spain, September 20, 2018, Proceedings 4*, 3–11. Springer.

## Appendix

### Temporal Stability Analysis

The proposed **Refined Temporal Pyramidal Compression-and-Amplification (RTPCA)** transformer effectively mines the intra&inter-block information from the attention mechanism, enhancing the model’s robustness compared to methods solely employing stacked spatial-temporal transformers. The cross-layer refinement module incorporated into our model fosters a deeper interaction, acting as a highly innovative fusion strategy. To assess the enhancements made on the temporal transformer, we performed a temporal stationary analysis experiment. As depicted in Figure 4, we measured the frame-wise Mean Per Joint Position Error (MPJPE) on the Human3.6M test set, with subjects S9 and S11 performing the *Photo* action. The frame-wise MPJPE represents the average error of all estimated joints in each frame. The shaded area in the figure signifies the range of maximum and minimum values across the test samples, with the middle line illustrating the average. The green and red lines represent the MPJPE over 600 frames for our method and the current SOTA method (MixSTE), respectively. The results demonstrate that our method exhibits less fluctuation and lower MPJPE values, showcasing its stability and accuracy over the MixSTE method.

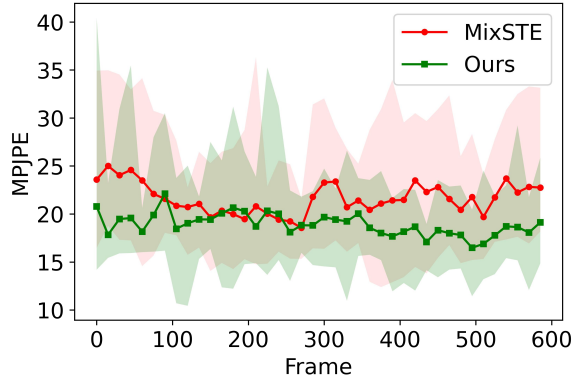


Figure 4: **The MPJPE-Frame curves using MixSTE and our methods.** The comparison of the proposed method and MixSTE on Human3.6M test set using frame-wise MPJPE for *Photo* action is conducted and our method outperforms MixSTE with higher accuracy and stability.

### Attention Visualization

To validate that the proposed RTPCA is capable of efficiently utilizing connections for information aggregation and exploring the attention mechanism, we conducted an attention visualization experiment, as demonstrated in Figure 5. Our model and MixSTE were evaluated on the Human3.6M test set S11 with the *Sitting* action, and the attention matrix of the second temporal transformer was visualized. The first and second rows of Figure 5 represent the visualization results of our method and MixSTE, respectively. Each attention matrix has a dimension of  $F \times F$  ( $F = 243$ ), and this heatmap reflects

the weighted relationship between every frame. Brighter colors signify higher attention scores, which are normalized in this figure. Through RTPCA, a more comprehensive understanding of attention can be obtained, whereas the original ST seems to focus predominantly on specific frames.

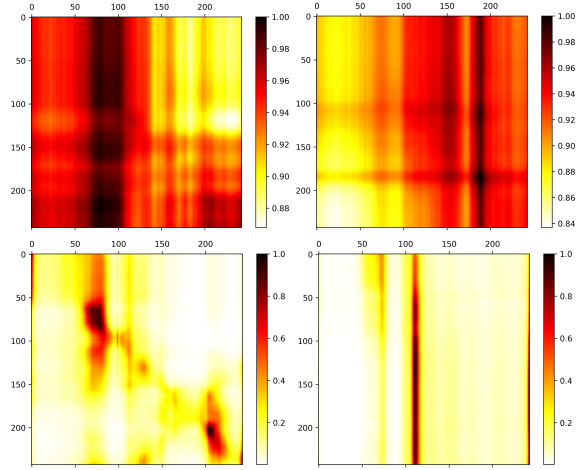


Figure 5: **Attention Visualization for our method and MixSTE.** The first row is the results of our method and the second row is the results of MixSTE. More comprehensive attention can be learned using our method which testifies the effectiveness to aggregate information. The original ST tends to focus on certain frames.